Icarus 316 (2018) 128–139

Contents lists available at ScienceDirect

Icarus

journal homepage: www.elsevier.com/locate/icarus

The geology of the occator quadrangle of dwarf planet Ceres: Floor-fractured craters and other geomorphic evidence of cryomagmatism

D.L. Buczkowski[a,*], D.A. Williams[b], J.E.C. Scully[c], S.C. Mest[d], D.A. Crown[d], P.M. Schenk[e], R. Jaumann[f], T. Roatsch[f], F. Preusker[f], A. Nathues[g], M. Hoffmann[g], M. Schaefer[g], S. Marchi[h], M.C. De Sanctis[i], C.A. Raymond[c], C.T. Russell[j]

[a] JHU-APL, Laurel, MD, USA
[b] School of Earth & Space Exploration, Arizona State University, Tempe, Arizona, USA
[c] NASA JPL, California Institute of Technology, Pasadena, California, USA
[d] Planetary Science Institute, Tucson, Arizona, USA
[e] LPI, Houston, Texas, USA
[f] DLR, Berlin, Germany
[g] MPI Solar System Research, Göttingen, Germany
[h] Southwest Research Institute, Boulder, Colorado, USA
[i] National Institute of Astrophysics, Rome, Italy
[j] UCLA, Los Angeles, California, USA

ARTICLE INFO

Article history:
Received 24 October 2016
Revised 10 May 2017
Accepted 31 May 2017
Available online 7 June 2017

ABSTRACT

The Dawn Science Team is conducting a geological mapping campaign at Ceres during the nominal mission, including iterative mapping using data obtained during each orbital phase. We are using geological mapping as a method to identify the geologic processes that have modified the surface of dwarf planet Ceres. We here present the geology of the Ac-9 Occator quadrangle, located between 22°S-22°N and 216-288°E. The Ac-9 map area is within the topographically high region named Hanami Planum. Features of note within the profile include impact craters Occator, Azacca, Lociyo, Nepen and Kirnis. Four of these craters have fractured, shallow floors, morphometrically comparable to floor-fractured craters (FFCs) on the Moon. Similar to models for the formation of the lunar FFCs, we suggest that these Ceres FFCs are a result of cryomagmatic uplift under the crater floors. A set of regional linear structures called the Samhain Catenae do not have any obvious relationship to impact craters. Many of the catenae are comprised of smaller structures that have linked together, suggestive of en echelon fractures. It has been suggested that these fractures formed due to the uplift of Hanami Planum due to cryromagmatic plumes.

1. Introduction

NASA's Dawn spacecraft (Russell and Raymond, 2011) was captured into orbit by the dwarf planet Ceres on March 6, 2015. During the Approach phase, capture was preceded and followed by a series of optical navigation and rotation characterization observations by Dawn's Framing Camera (FC) (Sierks et al., 2011), which provided the first images of Ceres' surface. Data were acquired at progressively lower altitudes, resulting in increased spatial resolutions: late Approach (1.3 km/px), Survey orbit (415 m/px), the High Altitude Mapping Orbit (HAMO—140 m/px) orbits, and the Low Altitude Mapping Orbit (LAMO—35 m/px).

As was done at Vesta (Yingst et al., 2014), the Dawn Science Team is conducting a geological mapping campaign at Ceres, to identify the geologic processes that have modified the surface of the dwarf planet. We utilize an iterative mapping process, using data obtained during each orbital phase. The mapping campaign includes a 1:10 M global map of Ceres based on Survey data (Buczkowski et al., 2016), a 1:1 M global map based on HAMO imagery (*Mest* and co-workers, this issue), and a series of fifteen 1:500 K quadrangle maps (Fig. 1a), based on LAMO imagery (Williams et al., *this issue (Intro paper)*). We here present the geology of the Ac-9 Occator quadrangle, located between 22°S-22°N and 216–288°E (Fig. 1).

* Corresponding author.
E-mail address: debra.buczkowski@jhuapl.edu (D.L. Buczkowski).

http://dx.doi.org/10.1016/j.icarus.2017.05.025
0019-1035/

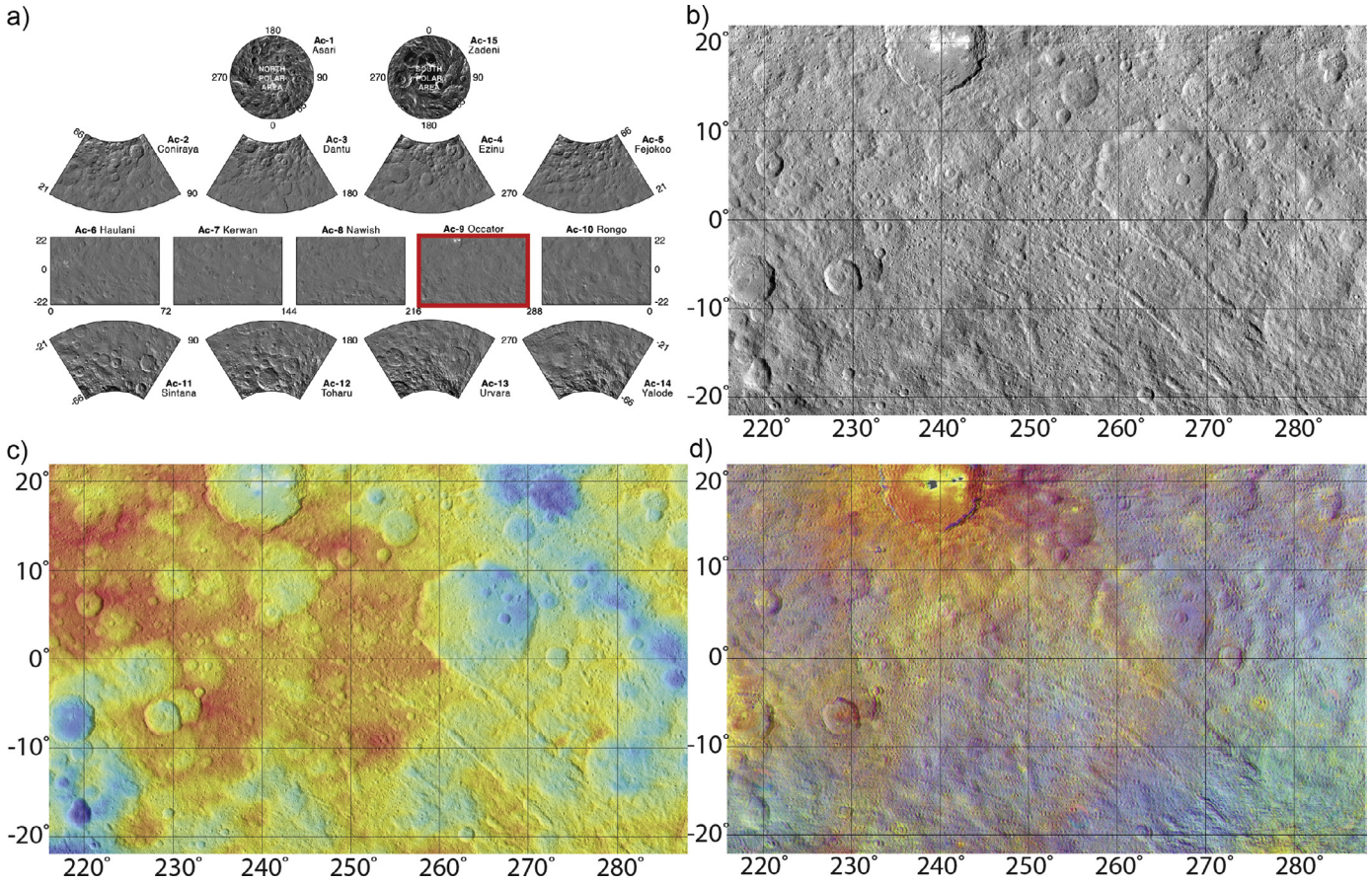

Fig. 1. The Ac-9 Occator quadrangle of Ceres. a) Quadrangle scheme for Ceres. Ac-9 is outlined in red. b) LAMO resolution (~35 m/pixel) FC clear filter (monochromatic) mosaic of the Occator quadrangle. c) Stereo-photogrammetric HAMO digital terrain model of Ac-9, overlying the LAMO mosaic. d) FC color composite mosaic of the Occator quadrangle. R: 750/965 nm, G; 750 nm, B: 750/440 nm. (For interpretation of the references to color in this figure legend, the reader is referred to the web version of this article.)

2. Data

The Framing Camera observes Ceres with a clear filter and 7 band-pass filters covering the wavelengths from the visible to the near-IR (Sierks et al., 2011). Clear filter (monochrome) FC LAMO images (spatial resolution of ~35 m/pixel) were mosaicked (Fig. 1b) to make a base for the Ac-9 Occator quadrangle. Analysis of the Ac-9 imagery was enhanced by observation of the quadrangle's topography (Fig. 1c). A digital terrain model (DTM) of Ceres (vertical accuracy ~15 m) was derived stereophotogrammetrically from HAMO orbit FC data (spatial resolution of ~140 m/pixel) (Preusker et al., 2016). This topography was continuously improved as the spatial resolution of the FC data steadily increased due to Dawn's three-tier orbital phasing.

Variations in the surface compostion were revealed using FC color ratio images using standard ratios [Red (750/970 nm) represents stronger absorptions at longer (near-IR) wavelengths; Green (750 nm) captures albedo variations; Blue (750/440 nm) represents stronger absorptions at shorter (visible) wavelengths]; the spectral and compositional diversity of crater ejecta materials within the quadrangle is illustrated by the strong variations present in the color-ratio composite image (Fig. 1d). Evaluation of VIR data was then performed to investigate the significance of these color variations.

3. Geologic setting and key features

Geomorphic features identified on Ceres include impact craters, linear structures, domical features and lobate flows (Buczkowski et al., 2016). The lack of a large inventory of relaxed craters (Hiesinger et al., 2016), the presence of ancient surface fractures (Buczkowski et al., 2016), and extensive sub-surface fracturing (as demonstrated by the widespread distribution of polygonal craters) (Buczkowski et al., 2016), suggests that the crust is too strong to be dominated by ice. However, the main components of the Ceres crust have been determined to be rock, ice, and salt hydrates (Russell et al., 2016), including carbonates (DeSanctis et al., 2015, 2016) and ammoniated phyllosilicates (DeSanctis et al., 2015; Ammanito et al., 2016), and a crust of this composition has been shown to be strong enough (Durham et al., 1992) to support the observed geomorphic features.

The Ac-9 Occator quadrangle is located in the equatorial region of Ceres, extending from ±22.5 latitude, and from 216-288°E longitude (Fig. 2, black dashed rectangle). The map area is dominated by Hanami Planum, an elevated region of the dwarf planet, and the quadrangle is named for Occator crater, the brightest region on Ceres. Many of the impact craters in Ac-9 have fractured floors that are consistently shallow compared to similarly-sized non-fractured craters. The quadrangle region is also crossed by a set of kilometer long linear structures, named the Samhain Catenae. We here discuss the several noteworthy features in the Ac-9 quadrangle.

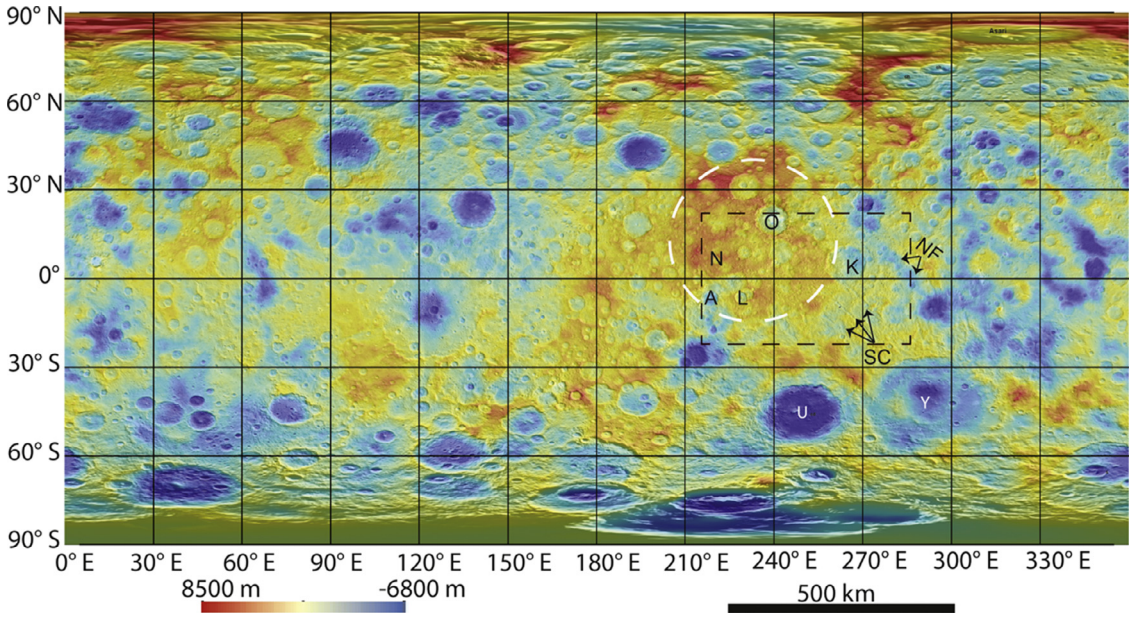

Fig. 2. Stereo-photogrammetric digital terrain model of Ceres (displayed in simple cylindrical projection), overlying the LAMO global mosaic. Heights are relative to the triaxial ellipsoid dimensions (482 × 482 × 446 km). The white dashed circle outlines Hanami Planum. Black dashed rectangle shows the location of Ac-9 quadrangle. Features of note within the quadrangle are labeled (O = Occator; A = Azacca; L = Lociyo; N = Nepen; K = Kirnis; NF = Nabanna Fossa; SC = Samhain Catenae), as are the Urvara (U) and Yalode (Y) basins.

3.1. Hanami Planum

The western portion of the Ac-9 map area is within the topographically high region named Hanami Planum (Fig. 2, white dashed circle). Centered at 15°N, 230°E, Hanami Planum is the only discrete topographically high region on Ceres (Buczkowski et al., 2016). It is one of two longitudinally distinct regions where European Space Agency (ESA) Herschel Space Observatory data suggested a release of water vapor (Küppers et al., 2014). The strongest negative Bouguer anomaly on Ceres is associated with Hanami, which suggests that there is either a relatively low regional density, or there is a buoyancy-driven anomaly beneath the planum (Ermakov et al., 2017). Geodynamic modeling suggests that the Hanami region could be topographically high due to upwelling of sub-surface material (King et al., 2016; Scully et al., 2016).

3.2. Impact craters

Impact craters are the most prevalent geomorphic feature on Ceres (Hiesinger et al., 2016; Buczkowski et al., 2016). It was predicted that most craters on Ceres would be relaxed (Bland., 2013), with shallow floors and little to no rim. Instead many of Ceres' craters are unrelaxed or only partially relaxed (Hiesinger et al., 2016), with sharp walls and deep floors compared to what was predicted by Bland et al. (2013). The craters in Ac-9 show no evidence of being relaxed.

3.2.1. Occator crater

Occator crater is a 92 km diameter impact crater centered at 19.8°N, 239.3°E (Fig. 2). The crater walls are terraced and the rim is scalloped, with multiple 90° bends and straight segments (Fig. 3a). From rim to floor, the crater has 3.5 km of relief (Fig. 3b). A 9 km wide, ~1 km deep central pit is located in the center of the crater, with a 2 km wide, ~400 m high central dome on its floor (Fig. 3c) (Schenk et al., 2015; Hiesinger et al., 2016; Buczkowski et al., 2016). While Occator's floor material ranges from smooth to knobby, and embays the terraced wall material, in the northeast it is overlain by lobate flows (Fig. 3e, f) whose margins suggest that they may emanate from the center of the crater (Krohn et al., 2016).

The floor of Occator crater is extensively fractured (Fig. 3d). Floor fractures include: (1) Linear fractures crossing the floor from SW toward the central pit; (2) Linear fractures crossing the lobate flow in the NE; (3) Concentric fractures encircling its central pit; and (4) Concentric fractures at the base of the crater wall. A pattern of cross-cutting fractures cut both the SSW crater wall and floor; this fracture set shows apparent broad outer arc extension, with at least two central peaks, and a transition to radial faulting with distance from the center. In addition to these several sets of floor fractures, there are also concentric fractures high on the crater wall, near the crater rim, and fractures exterior to the crater in its ejecta blanket that are circumferential to the Occator rim.

In the color ratio image of Ac-9, the Occator ejecta is comprised of multiple colors (Fig. 1d). Changes of "color" correspond to changes in albedo evident in the clear filter data (Fig. 1a) and generally related to changes in ejecta morphology.

Anomalously bright features have been observed on Ceres, both by the Hubble Space Telescope (Li et al., 2006) and by Dawn (Nathues et al., 2015). The brightest of these features occur on the center and northeastern floor of Occator (Fig. 3c, e). These bright materials coincide with where observations by the Herschel Space Observatory suggested water vapor emission from Ceres (Küppers et al., 2014). Ceralia Facula, the largest of the bright deposits, is associated with the dome within Occator's central pit (Schenk et al., 2016) and has distinct lobate margins (Fig. 3c). The Vinalia Faculae are comprised of multiple bright spots that are strongly associated with fractures cutting the NE lobate flows; unlike Ceralia Facula (Fig. 3f), these deposits have wispy margins (Fig. 3e). Both sets of faculae are comprised of sodium carbonates, which is a mineral detection unique to Occator crater (DeSanctis et al., 2016).

3.2.2. Azacca crater

Azacca is a 50 km diameter crater located at 6.7°S, 218.4°E (Fig. 2). The crater has a central ridge, wall terraces (Fig. 4a) and is ~2.6 km deep (Fig. 4b). Although not as extensively fractured as Occator, Azacca has both floor fractures and circumferential

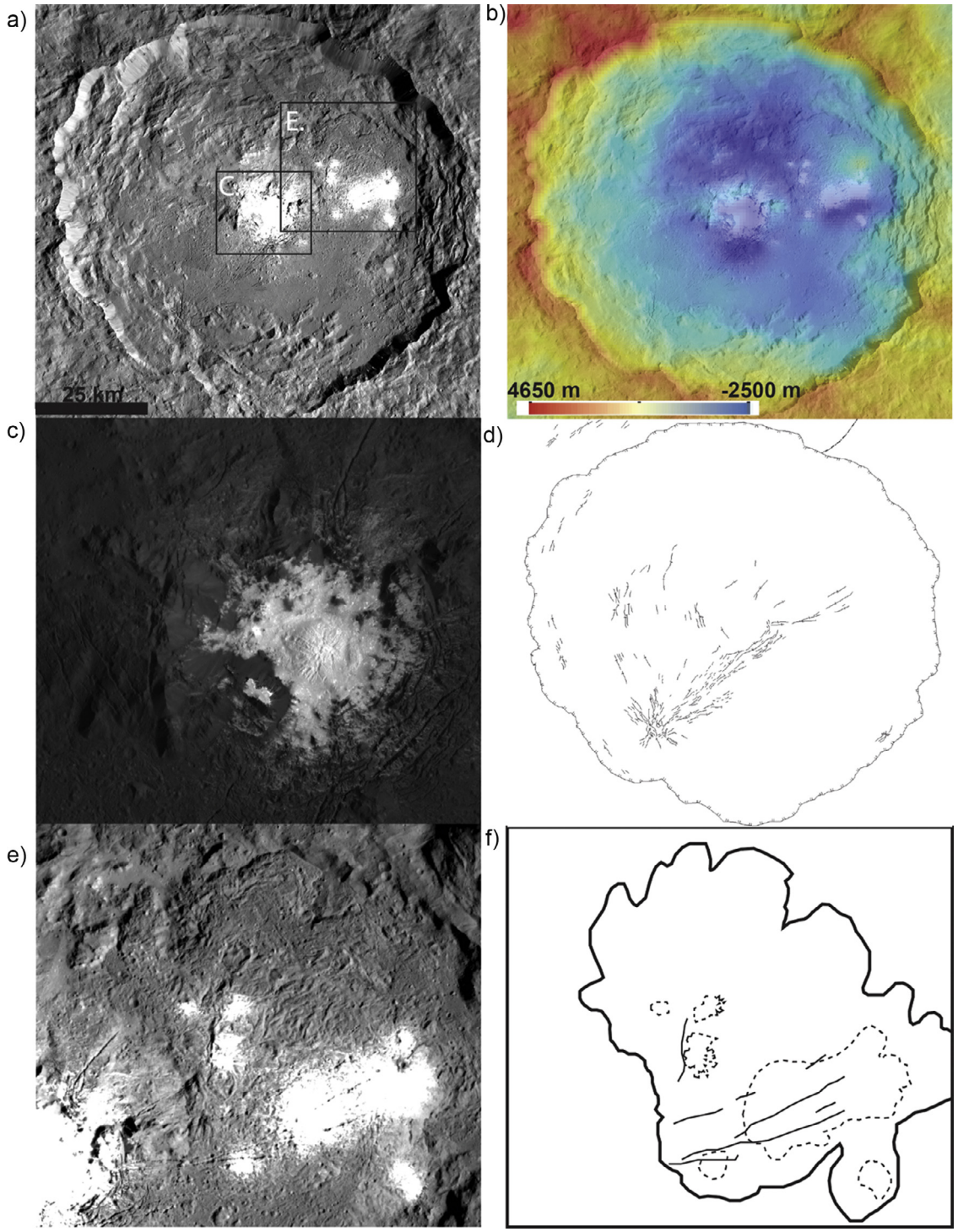

Fig. 3. a) FC clear filter LAMO mosaic (35 m/pixel) of Occator crater, centered at 19.8°N, 239.3°E. Boxes show the location of regions shown at full resolution in other figures. b) HAMO topography overlying LAMO clear filter image. c) Full resolution zoom of Occator's central pit and the dome on its floor. The association of the central pit with the bright material is visible. d) Fracture map of Occator crater. e) Full resolution zoom of the lobate flows on the floor of Occator. The association of the bright spots with the fractures is visible. f) Cartoon showing margins of lobate flow in e (thick solid line), the fractures on the flow (thin solid line), and the Vinalia Faculae (dashed lines).

fractures in its ejecta and crater walls (Fig. 4c). The majority of the floor fractures are linear fractures crossing roughly north to south, but there are also a few subtle fractures where the crater wall meets the floor (Fig. 4c). Also like Occator, the Azacca ejecta is multi-colored in the color ratio data (Fig. 1d), with changes in "color" corresponding to variable morphology. There are also bright spots on its floor and within its ejecta.

3.2.3. Lociyo crater

Lociyo is a 37.8 km diameter crater located at 6.5°S, 228.8°E (Fig. 5a). The floor of Lociyo is hummocky, with subtle, non-linear fractures (Fig. 5a). There is a central peak although it is only evident in the topographic data (Fig. 5b). The walls of Lociyo are not terraced and show little evidence of mass-wasting (Fig. 5a). From rim to floor, Lociyo has 2.2 km of relief (Fig. 5c).

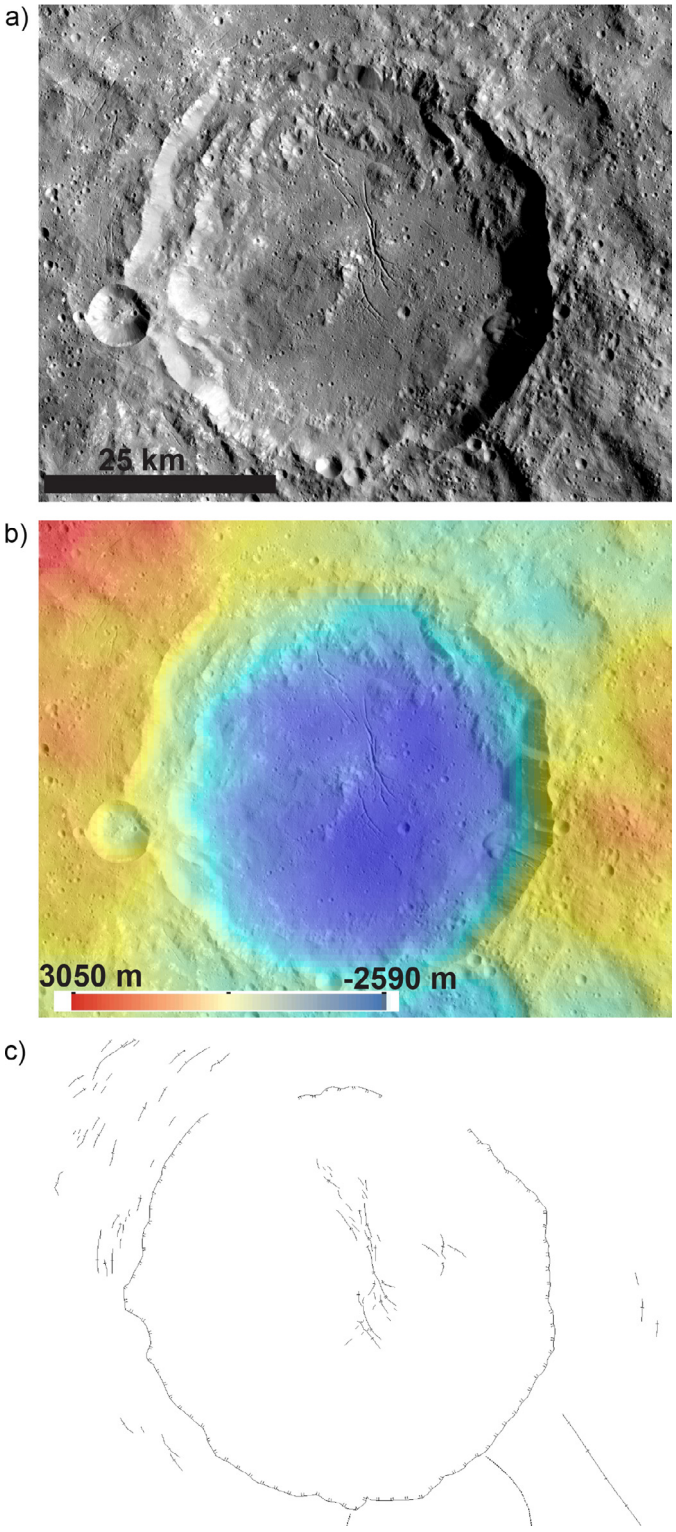

Fig. 4. a) FC clear filter LAMO mosaic (35 m/pixel) of Azacca crater, centered at 6.7°S, 218.4°E. b) HAMO topography overlying LAMO clear filter image. c) Fracture map of Azacca crater.

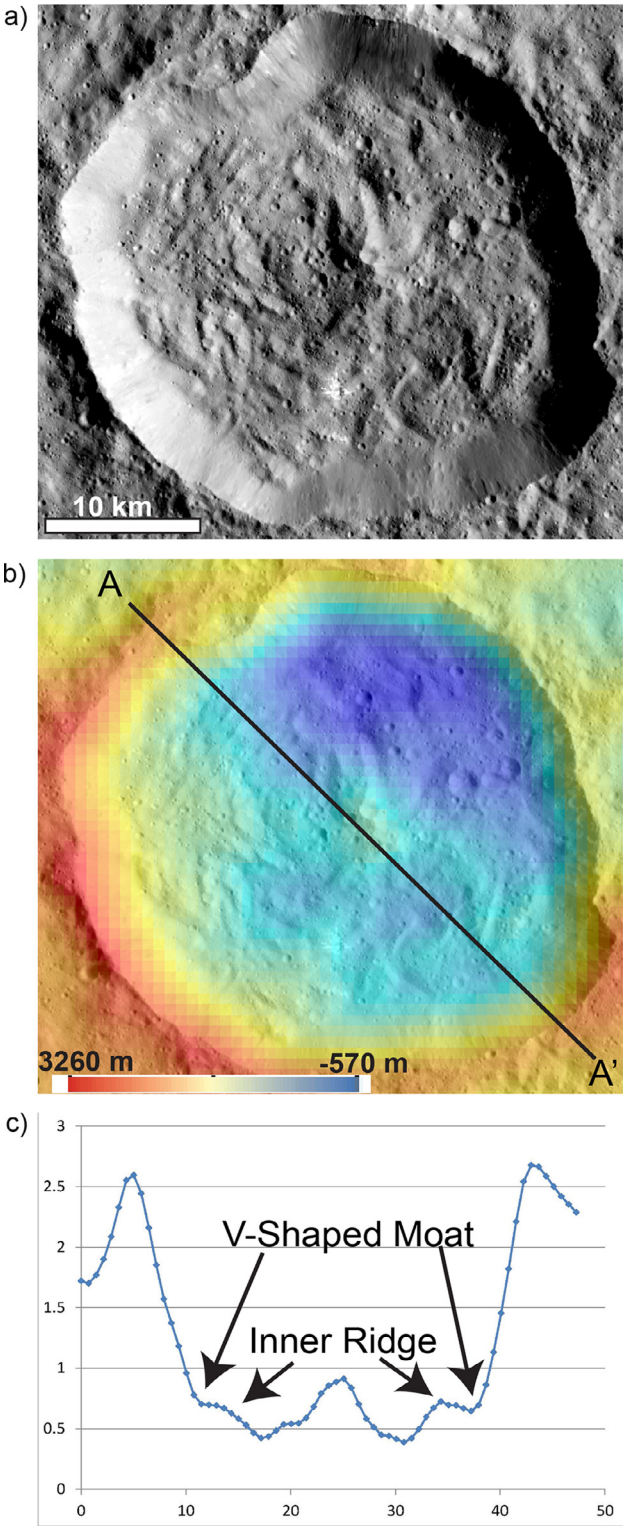

Fig. 5. a) FC clear filter LAMO mosaic (35 m/pixel) of Lociyo crater, centered at 6.5°S, 228.8°E. b) HAMO topography overlying LAMO clear filter image. A-A' line shows location of topographic profile displayed in part c. c) Topographic cross-section of Lociyo crater. V-shaped moats and interior ridges are marked.

Topographic profiles of Lociyo show that there are v-shaped moats separating the crater floor from the crater walls (Fig. 5c). There is an inner ridge of material, where the crater floor is topographically high relative to the either the moat or the area closest to the central peak (Fig. 5c). This moat-ridge topography is not observed in either Occator or Azacca.

3.2.4. Nepen crater

Nepen is a 26.4 km diameter crater located at 6.2°N, 220.5°E (Fig. 2). The floor of Nepen is more heavily cratered that Occator, Azacca or Lociyo, although it displays a sharp rim with little evidence of post-formation mass-wasting (Fig. 6a). There is a central ridge and the crater walls are not terraced (Fig. 6a). Nepen is

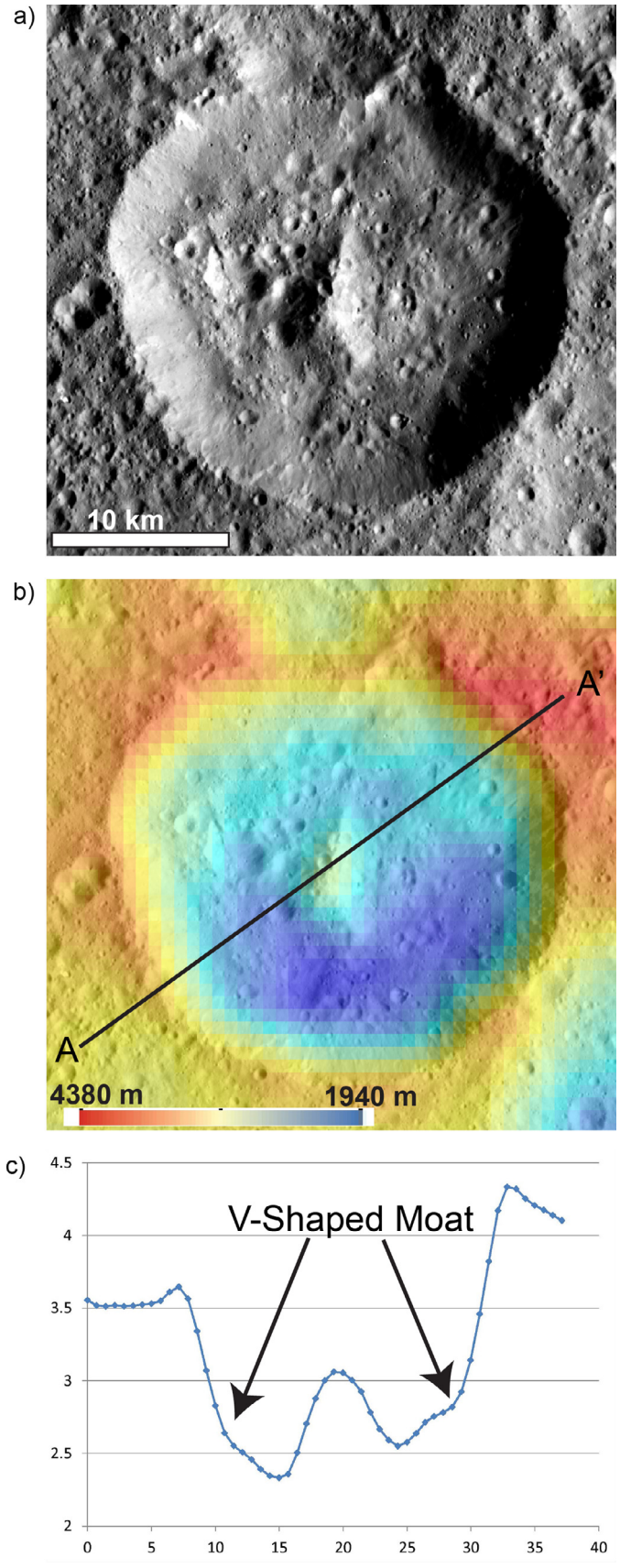

Fig. 6. a) FC clear filter LAMO mosaic (35 m/pixel) of Nepen crater, centered at 6.2°N, 220.5°E. b) HAMO topography overlying LAMO clear filter image. A-A' line shows location of topographic profile displayed in part c. c) Topographic cross-section of Nepen crater. Location of v-shaped moats are marked.

~1.6 km deep, from rim to floor (Fig. 6b). Like Lociyo, topographic profiles of Nepen show that there is a subtle moat where the crater floor meets the crater wall, although there is no (or only a very subtle) inner ridge (Fig. 6c).

3.2.5. Kirnis crater

Kirnis is a 115 km diameter crater located at 4.9°N, 264.3°E (Fig. 2). While Occator, Azacca, Lociyo, and Nepen are all relatively fresh craters with sharp rims, Kirnis appears to be more heavily degraded (Fig. 7a). The floor of Kirnis is more heavily cratered than the other named craters in Ac-9, and its depth from rim to floor is 4 km (Fig. 7b).

Kirnis is somewhat polygonal in shape, with multiple 90° bends and straight segments (Fig. 7a). Its southwestern rim is visibly deformed by a series of merged pits (Fig. 7a), one of the Samhain Catenae pit crater chains (see Section 3.3.1). Another Samhain Catena is located immediately to the northeast of the crater, and the northeastern portion of the rim is both straight and parallel to the pit chain (Fig. 7a).

The western floor of Kirnis is noticeably higher than the eastern floor (Fig. 7a,b). This high region is located partially on the Kirnis wall and is domical in shape across-slope (Fig. 7c). While it appears to be covered with secondary craters from Occator, it does not seem to be a deposit of Occator ejecta. There is a moat of low topography to the north of the dome (Fig. 7c) that would not be expected from an ejecta deposit originating from Occator crater, which is northwest of Kirnis (Fig. 2). The along-slope topographic profile is dominated by the overall trend of the crater wall (Fig. 7d) but the dome can be observed in topography data as standing above the rest of the wall (Fig. 7d), suggesting that it is not a mass-wasting deposit.

3.3. Linear structures

Linear structures—including grooves, pit crater chains, fractures and troughs—cross much of Ceres. Some of these structures appear to be radial to the large basins Urvara and Yalode, and most likely formed due to impact processes (Buczkowski et al., 2016). However, there are also kilometer-scale linear structures that do not have any obvious relationship to impact craters and may represent internally driven tectonics (Buczkowski et al., 2016). The majority of these structures are located within Ac-9.

3.3.1. Samhain Catenae

The Samhain Catenae (Fig. 8a) include seventeen linear assemblages of small merged depressions. Individual catena range in length from 28 km to over 200 km in length, and in depth from 100 to 450 m (Fig. 8b). Some of the catenae are cross-cut by grooves radial to the Urvara basin (Fig. 8c, dashed lines).

The lack of raised rims on the merged pits of the Samhain Catenae (Fig. 8a) makes it unlikely that these are secondary crater chains. Instead, the morphology of the Samhain Catenae more closely resembles that of pit crater chains, a type of feature identified on many planetary bodies, including Earth (Sigurdsson, 1980; Angelier et al., 1997; Okubo and Martel, 1998; Abelson et al., 2003), Mars (Wyrick et al., 2004; Ferrill et al., 2004), Enceladus (Michaud et al., 2008; Martin and Kattenhorn, 2013, 2014), Eros (Buczkowski et al., 2008) and Vesta (Buczkowski et al., 2014). There is a strong correlation between pit crater chains and fault-bounded graben on Mars (Wyrick et al., 2004) and they have been hypothesized to represent buried normal faults on a number of small bodies (Buczkowski and Wyrick, 2014). The theory suggests that dilational motion along the buried fault causes overlying material to collapse into the openings along its length (Horstman and Melosh, 1989; Sims et al., 2003; Wyrick et al., 2004). The individual pits can then merge together to form merged pits and even-

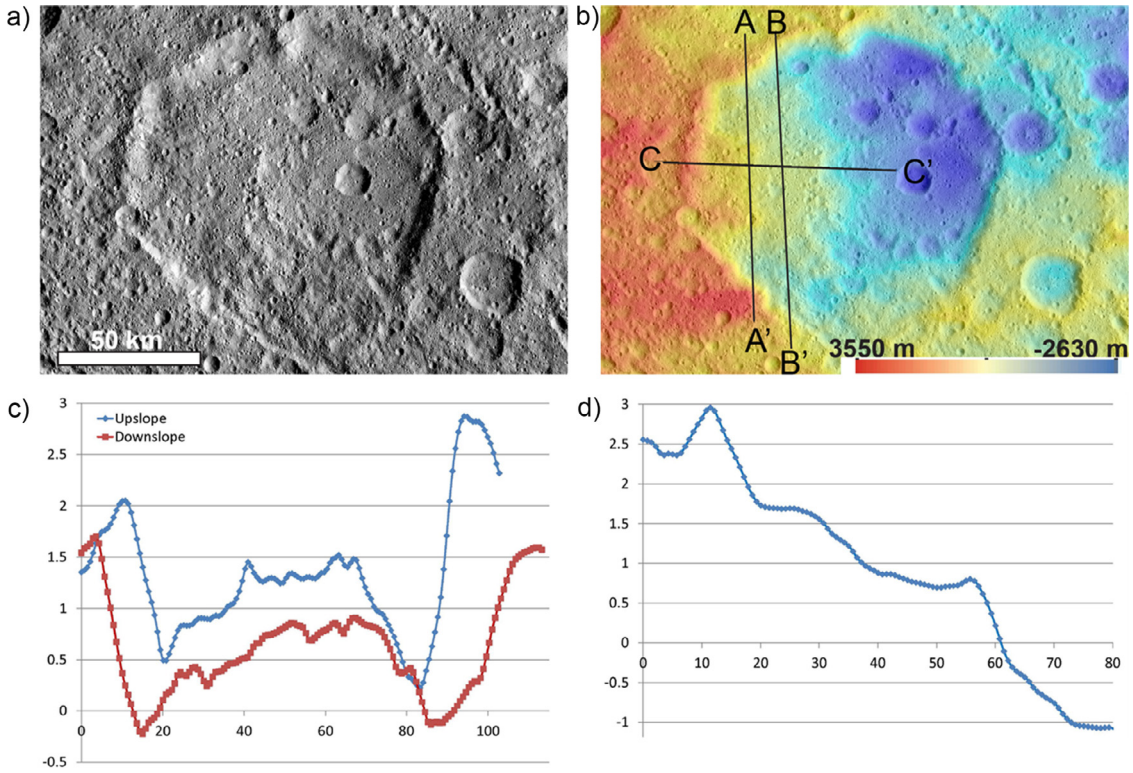

Fig. 7. a) FC clear filter LAMO mosaic (35 m/pixel) of Kirnis crater, centered at 4.9°N, 264.3°E. b) HAMO topography overlying LAMO clear filter image. A-A', B-B' and C-C' lines show the locations of topographic profiles displayed in parts c and d. c) Topographic cross-sections A-A' and B-B' of the dome in Kirnis crater. These cross-sections are taken across-slope to better display the dome-shaped profile of the topographically high region of Kirnis. d) Topographic cross-section C-C' of the dome in Kirnis. This cross-section was taken downslope.

tually grooves as the feature matures (Wyrick et al., 2004). This maturation of pit crater chains is a probable cause for the occasional groove and merged pits found among the Samhain Catenae (Fig. 8a).

By mapping the Samhain Catenae directly onto the Ceres shape model, and modeling them as planes that cut through the dwarf planet, an approximate strike and dip for the underlying faults were determined (Buczkowski et al., 2016). Clustering of the pole directions suggests that the Samhain Catenae represent similarly oriented planes (Fig. 8d), which implies a common formation mechanism of the corresponding structures. In similar analyses of linear structures on Vesta (Jaumann et al., 2012) and Eros (Buczkowski et al., 2008), the coordinates of the pole cluster correlated to an impact crater, which was then theorized to have produced the impact stresses that caused the faults to form; a similar orientation of structures to impact craters was observed on Ida (Asphaug et al., 1996) and Lutetia (Thomas et al., 2012). However, there is no visible impact crater at the coordinates where the poles of the Samhain Catenae cluster, reducing the likelihood that they formed due to impact stresses (Buczkowski et al., 2016).

3.3.2. Nabanna fossa

Nabanna Fossa is a 168 km long, 2.5 km deep degraded trough that extends from the northwest to the southeast on the eastern edge of the Ac-9 region (Fig. 9a). While Nabanna Fossa is not easily observable in the LAMO clear filter data (Fig. 9a), the linear depression is clearly visible in the HAMO topography (Fig. 9b). Pit crater chains from the Samhain Catenae border Nabanna on both sides, and are oriented similarly. Indeed, a planar analysis of Nabanna shows that it has a pole that clusters with those of the catenae (Fig. 8d, white star). This suggests that although Nabanna is morphologically different from the Samhain Catenae, they might share the same formation event.

4. Geologic mapping

Fig. 1 shows the LAMO base map, DTM, and color ratio composite mosaics for the Occator map region, while Fig. 10 shows our geological map and map legend. Because Occator crater crosses into the Ac-4 Ezinu quadrangle and Azacca crater crosses into the Ac-8 Nawish quadrangle, our mapping extends into these regions, irrespective of quadrangle boundaries. The Occator quadrangle itself is located between 22°S-22°N and 216-288°E

The central part of the quadrangle is dominated by a cratered terrain, which is covered by the ejecta blankets of Occator, Azacca, Lociyo and Nepen craters. Albedo and color data indicates that the ejecta from these craters have multiple colors, suggesting excavation of materials of different compositions. To the south in the quadrangle, the background cratered terrain is superposed by ejecta from the Yalode and Urvara basins.

In this section we give the description of map units (DOMU) for the Occator quadrangle map region. These map units are divided into regional map units and crater interior materials.

4.1. Regional map units

These are the units that cover large areas of Ceres. They include (1) cratered terrain, (2) smooth material, and (3) crater material.

4.1.1. Cratered terrain (ct)

Cratered terrain (ct) is the most widespread unit on Ceres. The material is heavily cratered at all crater diameters. Crater shapes range from round to polygonal, and crater rims vary from well

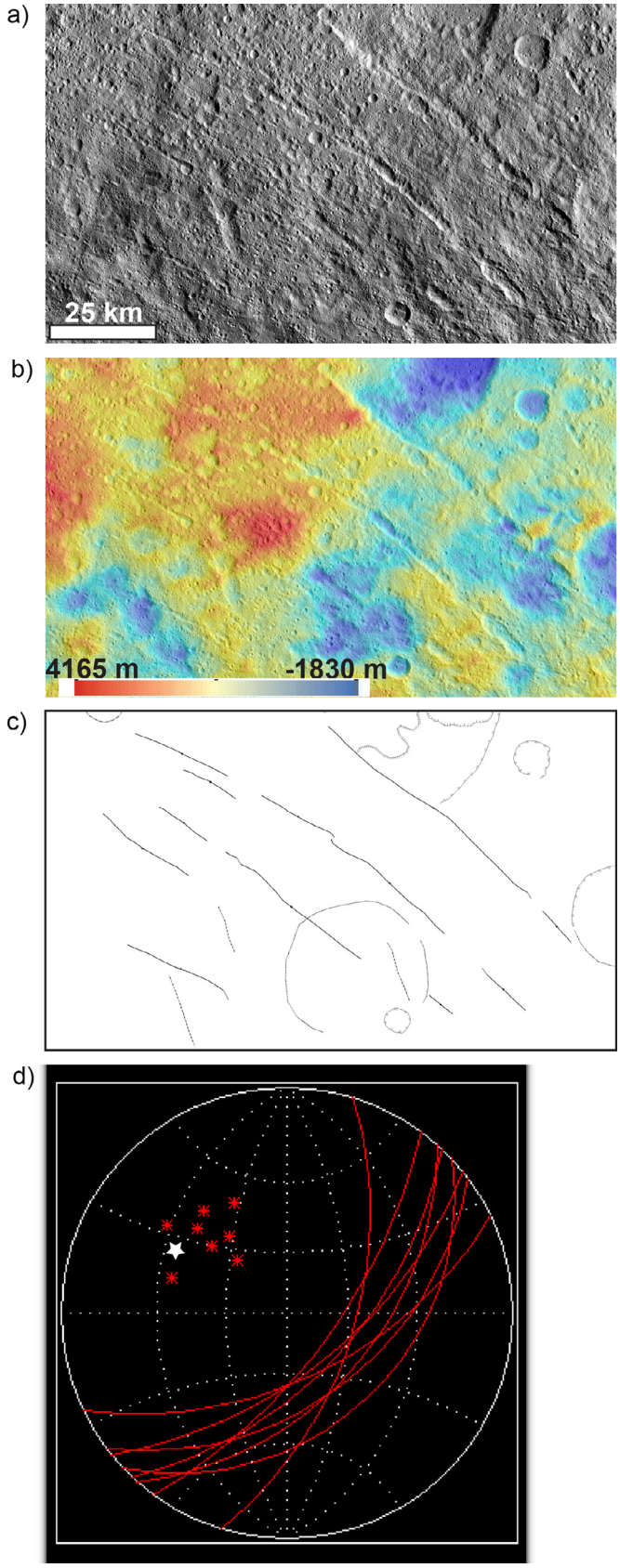

Fig. 8. a) FC clear filter LAMO mosaic (35 m/pixel) of the Samhain Catenae, extending from 21°S to 3°N, and from 237.9°E to 280.7°E. b) HAMO topography overlying LAMO clear filter image. c) Fracture map of the Samhain Catenae. Dashed lines represent grooves radial to Urvara that cross-cut the catenae. d) Stereonet plots of the Samhain Catenae. Pole positions cluster, centered at ~45°N, ~300°E. The white star represents the pole position of Nabanna Fossa.

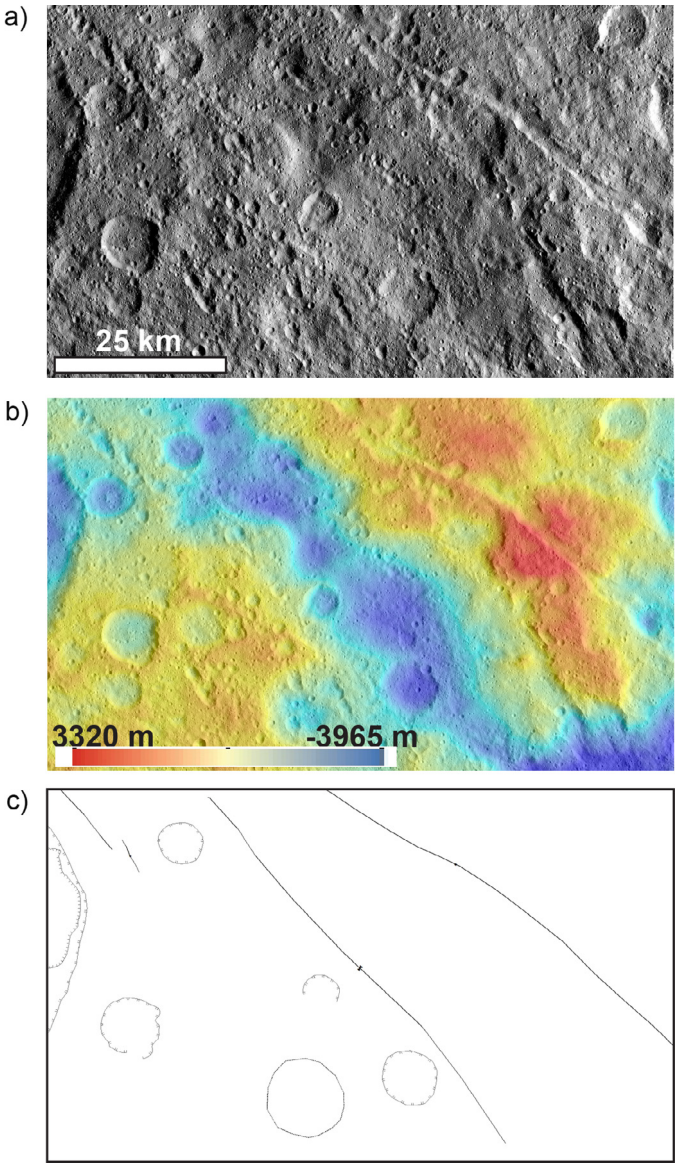

Fig. 9. a) FC clear filter LAMO mosaic (35 m/pixel) of Nabanna Fossa, centered at 3.0°N, 283.8°E. . b) HAMO topography overlying LAMO clear filter image. c) Fracture map of Nabanna Fossa and the adjacent Samhain Catenae.

preserved to almost completely missing. Crater floors are usually shallow and are superposed by ejecta from multiple directions. The DTM of Ceres shows that the unit has a variable relief that is typically hilly. The FC LAMO mosaic indicates that cratered terrain material is of generally low-albedo, with some minor variability; color ratio composite images show some subtle color variations, but in general the composition of Ceres surface does not vary from region to region (De Sanctis et al., 2016).

Cratered terrain is interpreted to be Ceres ancient crust, a composite of silicates, carbonates, and water ice (De Sanctis et al., 2016). All other units superpose the cratered terrain.

4.1.2. Smooth material (sm)

Smooth material (sm) shows the same albedo and color variations as cratered terrain, but has a lower abundance of larger craters. While smooth material shows variable relief, it in general is less hilly than the cratered terrain. At LAMO resolution there is no clear evidence for flow fronts, vents, or other structures in this unit.

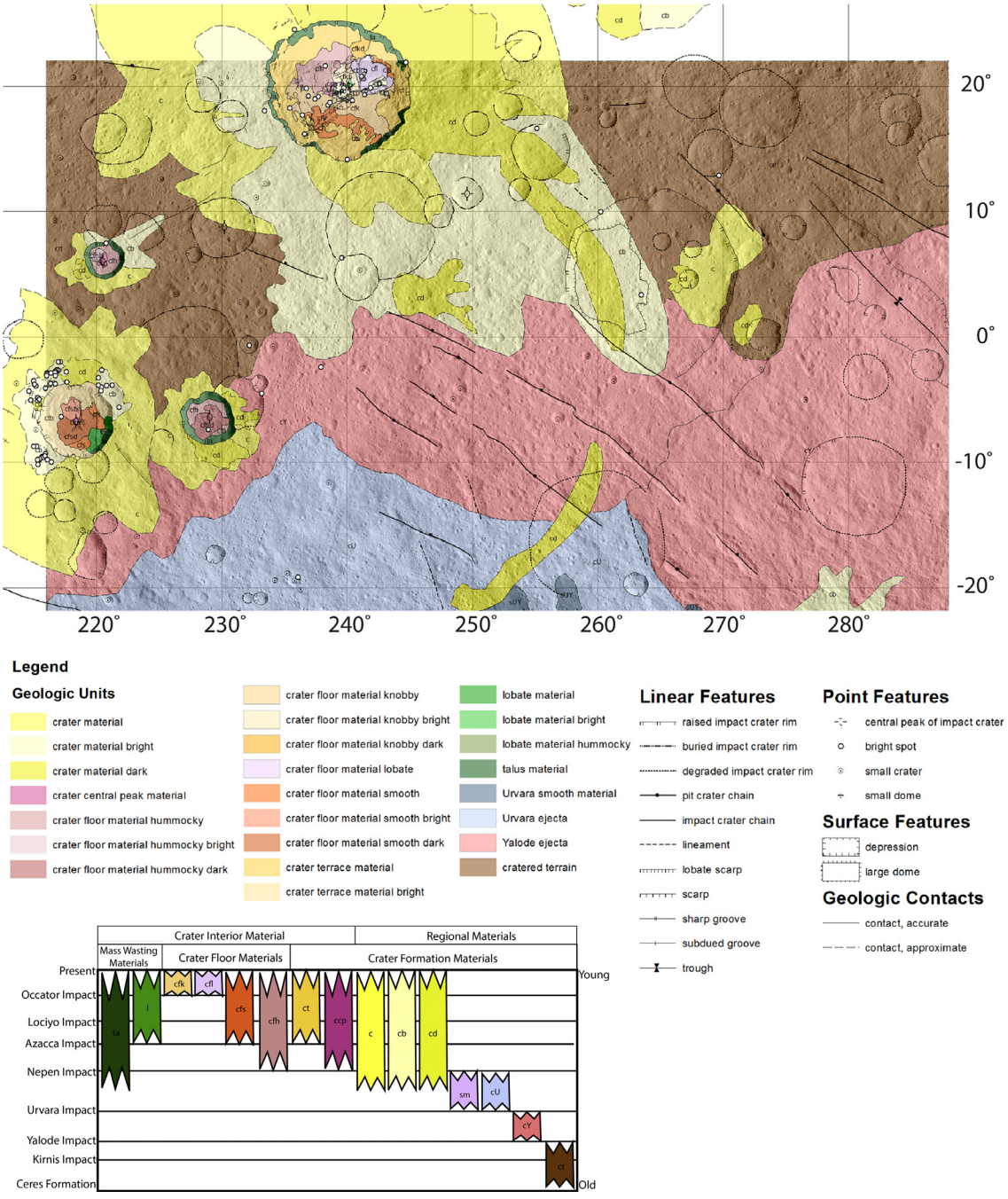

Fig. 10. The geologic map of the Ac-9 Occator quadrangle, based on LAMO data. The map, presented at 1:500 K scale, is displayed in simple cylindrical projection, with legend and correlation of map units (COMU).

Smooth material is interpreted to be re-melted cerean crustal material emplaced after large impact events. The smooth material in Ac-9 is the marginal end of a deposit extending from Urvara crater in quadrangle Ac-13 Urvara (Crown et al., this issue).

4.1.3. Crater material (c)

Crater material (c) is located within 1–2 crater diameters of large impact craters, such as Occator, Azacca, Lociyo and Nepen in this quadrangle. In some locations, the surface is marked by linear striations or chains of small impact craters radiating from the large impact crater. A variable morphology also marks this surface, from flat to hilly to hummocky, but with a sculpted appearance distinct from the underlying terrain. Crater material displays small impacts, but with a lower crater density than the cratered terrain.

Crater material around different craters can include variations in albedo and color ratio images. Large deposits of both high albedo *bright crater material* (cb) and low-albedo *dark crater material* (cd) are found around the large craters in Ac-9. In most cases, these albedo differences are more clearly observed in the color ratio images (Fig. 1d).

Following the convention established in the map of the Ac-13 Urvara and Ac-14 Yalode quadrangles (Crown et al., this issue), the crater material surrounding the Urvara and Yalode basins have been mapped as distinct units, *Urvara crater material* (cU) and

Yalode crater material (cY). While the *Urvara crater material* and the eastern deposit of *Yalode crater material* shares the morphology of other *crater material*, the western deposit of Yalode crater material does not. This part of the unit was mapped based on the boundary of the Low Crater Density (LCD) region that Hiesinger et al., (2016) theorized was caused by ejecta from the largeYalode basin; it is thus marked by an "inferred" unit contact.

Crater material is interpreted to be continuous ejecta radiating from centrally-located impact craters. It superposes cratered terrain, and thus is relatively younger. Differences in crater material albedo have been interpreted to reflect differences in the composition of excavated materials.

4.2. Crater interior materials

Four of the craters in Ac-H-9 (Occator, Azacca, Lociyo and Nepen) have complex interiors, with crater peaks, terraced walls and multiple crater floor units.

4.2.1. Smooth crater floor material (cfs)

Smooth crater floor material (cfs) consists of sparsely cratered material with few or no knobs found on crater floors. In Ac-9, cfs is identified in Occator and Azacca craters. In both craters, the smooth crater floor material hosts extensive fracturing. Smooth crater floor material embays higher standing crater materials, suggesting that it is emplacement by flows, although few flow fronts are observed. Changes in albedo are noted as *smooth crater floor material bright* (cfsb) and *smooth crater floor material dark* (cfsd). Smooth crater floor materials is interpreted to be impact melt.

4.2.2. Knobby crater floor material (cfk)

Knobby crater floor material (cfk) is comprised of sparsely cratered material on crater floors with a higher density of knobs than the smooth crater floor material. In Ac-9, cfk is found on the floor of Occator and Azacca craters. Changes in albedo are noted as *knobby crater floor material bright* (cfkb) and *knobby crater floor material dark* (cfkd). Knobby crater floor materials is interpreted to be impact melt with a significant impact breccia component.

4.2.3. Hummocky crater floor material (cfh)

Hummocky crater floor material (cfh) is comprised of a sparsely cratered material of uneven topography. It has been identified on the floors of Occator, Lociyo and Nepen craters. Differences in albedo are noted as *hummocky crater floor material bright* (cfhb) and *hummocky crater floor material dark* (cfhd). Hummocky crater floor material is interpreted to be crater floor material deformed by cryomagmatic upwelling beneath the crater.

4.2.4. Lobate crater floor material (cfl)

Lobate crater floor material (cfl) is found on the floor of Occator crater. This material shows no impact cratering, but is fractured and covered with diffuse patches of high albedo material in association with the fractures. The surface of the cfl is ropy in texture and is inflated relative to the rest of the crater floor. The margins of these floor materials are distinctly lobate and are oriented such as suggests that they emanate from the center of the crater. Lobate crater floor material is interpreted to be flow materials emplaced after the formation of the crater.

4.2.5. Central peak material (ccp)

Central peak material (ccp), mapped in Occator, Azacca and Nepen craters, is centrally-located material that stands higher than the rest of the crater floor. Although there is little difference in albedo between crater peak material and other crater floor materials, there are variations in the color ratio data that suggest that the central peak material might have a different composition. In Occator crater, the central peak material is located at the edges of the central pit. Crater peak material is interpreted to be deep crurstal material uplifted from depth by tectonism and impact-basin formation.

4.2.6. Crater terrace material (ct)

Crater terrace material (ct), found in both Azacca and Occator craters, is crater wall material that is broken into a series of terraces. Some of the terraces are flat-lying and wide, with steep ends leading to the next terrace, while others are more ridged in shape and planform. Crater terrace material is only very lightly cratered but is commonly superposed by both lobate material and talus material, indicating its relatively older age. In Occator crater, the crater terrace material host small fracture systems.

Crater terrace material is interpreted to have formed due to downward movement of the crater wall along a series of concentric faults that formed during impact crater formation. According to crater formation models (e.g. French, 1998) terrace formation occurs specifically during the collapse of the transient crater.

4.2.7. Lobate material (l)

Lobate material (l) is comprised of accumulations of material that have flowed down slope in a lobate manner. It is also identified as mounds of material located on crater floors. There is no apparent variation in albedo or color compared to the surrounding materials. Lobate material is interpreted to be surface material that has been transported downslope by mass wasting.

4.2.8. Talus material (ta)

Talus material (ta) includes deposits of smooth material with linear, downslope striations and very few small craters. It is found on the steep walls of fresh craters such as Occator, Azacca, Nepen and Lociyo, but not on the walls of degraded craters such as Kirnis. Talus material is interpreted to be surface material that has been transported downslope by mass wasting.

5. Discussion

Many of the impact craters on Ceres have been found to have patterns of fractures on their floors, similar to those observed in Occator and Azacca (Buczkowski et al., 2016). These craters have been compared to a class of lunar craters referred to as Floor-Fractured Craters (FFCs) (Schultz, 1976). Lunar FFCs have been classified into crater classes, Types 1 through 6, based on their fracture patterns and other morphometric properties (Schultz, 1976; Jozwiak et al., 2012, 2015). The depth versus diameter (d/D) relationship of the lunar FFCs is distinctly shallower than the same association for other craters on the moon (Schultz, 1976; Jozwiak et al., 2012, 2015). Models for FFC formation incorporate explanations of their anomalously shallow floors by invoking either floor uplift due to magmatic intrusion beneath the crater (Schultz, 1976; Jozwiak et al., 2012; Jozwiak et al., 2015), or floor shallowing due to viscous relaxation (e.g. Hall et al., 1981).

Buczkowski et al., (2016) cataloged the Ceres FFCs according to the classification scheme designed by Schultz (1976) and utilized by Jozwiak et al., (2012; 2015) and found that large (>50 km) craters are most consistent with Type 1 lunar FFCs. Following the lunar FFC classification scheme both Occator and Azacca are Type 1 craters, which are described as generally large craters with central peak complexes, extensive wall terraces, and radial and/or concentric fractures on their floors (Schultz, 1976). Both Occator and Azacca have terraced walls, and a central structure. As discussed in Section 3.2.1, Occator crater has several sets of fractures on its floor, including concentric fractures encircling the central pit, linear fractures crossing its floor, and concentric fractures close to the

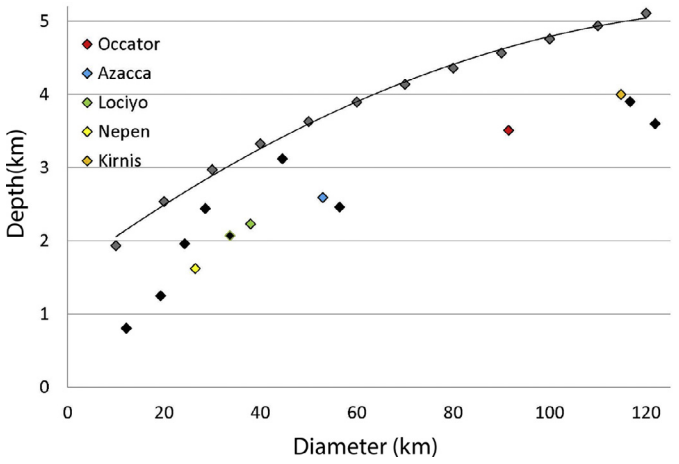

Fig. 11. Depth to diameter ratio of the floor fractured craters currently identified on Ceres, adapted from Buczkowski et al., (2016). Colored dots represent craters in the Ac-9 quadrangle, while black dots represent FFCs located elsewhere on Ceres. The black line is a second order polynomial fit to the depth to diameter ratio for the average Ceres crater as derived by Hiesinger et al., (2016).

crater wall (Fig. 3d). Azacca crater (Section 3.2.2) has primarily linear fractures crossing its floor, but there are also a few concentric fractures near its wall (Fig. 4c). Type 1 lunar FFCs were found by Jozwiak et al., (2012; 2015) to be most consistent with formation by magmatic intrusion, where an inflating domical sill (laccolith) beneath the crater floor uplifts the surface, causing fractures to form due to the deformation and shallowing the floor.

Other craters on Ceres are more consistent with Type 4 lunar FFCs (Buczkowski et al., 2016), which are defined by the presence of a v-shaped moat separating the wall scarp from the crater interior. The three sub-classes of Type 4 FFCs (4a, 4b, 4c) differ in the depth of the moat, whether there is an inner ridge associated with the moat, and on how pronounced the floor fractures are (Jozwiak et al., 2012). While neither Lociyo nor Nepen have obvious floor fractures, they do have v-shaped moats in their topographic profiles, indicative of Type 4 FFCs. Lociyo has a hummocky interior, with subdued grooves instead of sharp fractures (Fig. 5a), and its topographic profile shows v-shaped moats and interior ridges (Fig. 5c). These morphometric features are representative of a Type 4b FFC. Nepen crater, on the other hand, has the v-shaped moats (Fig. 6c), but no distinct interior ridge and a less hummocky floor; this makes Nepen more consistent with a Type 4c FFC. Type 4 lunar FCCs have also been found to be more consistent with formation due to magmatic uplift. Viscous relaxation models were unable to produce moats of any shape in the crater interiors (Hall et al., 1981; Dombard and Gillis, 2001), but in magmatic intrusion models a v-shaped moat marks the extent of the subsurface intrusion (Jozwiak et al., 2015).

The depth to diameter ratio of all Ceres craters was measured by Hiesinger et al., (2016); the second order polynomial fit to this d/D ratio (Schenk et al., 2016) allows us to derive the depth of the average Ceres crater of any particular diameter (Fig. 11, grey diamonds). An analysis of the d/D ratio of Occator, Azacca, Lociyo and Nepen craters show that they are anomalously shallow compared to the average Ceres crater (Fig. 11, colored diamonds), as are the other Ceres FFCs (Fig. 11, black diamonds, from Buczkowski et al., (2016)). This suggests that these craters may be experiencing an intrusion of a low-density material from below the craters that is uplifting their floors. While for lunar FFCs the intrusive material is hypothesized to be silicate magma (Schultz, 1976; Jozwiak et al., 2012, 2015), it has been suggested that cryomagmatic intrusions could be responsible for the formation of the Ceres FFCs (Buczkowski et al., 2016).

The floor-fractured craters in Ac-9 are not the only evidence of cryomagmatism in the quadrangle. The central pit/dome complex found in Occator crater might also be a geomorphic indication of crymagmatic activity. Large (>60 km diameter) craters on Ganymede and Callisto frequently have central pits with domes on their floors (Schenk, 1993). It has been hypothesized that the domes in these pits form due to either syn-impact uplift (Schenk, 1993; Bray et al., 2012) or post-impact diapirism (Moore and Malin, 1988) in craters that impacted where target materials were ice-rich. The similarity of the morphology of the Occator pit and dome to those seen in impact craters on Ganymede and Callisto is thus a further indication that cryomagmatism might be occurring under Occator.

Hanami Planum might also be a geomorphic expression of cryomagmatism, albeit on a much larger scale. Geodynamic modeling of convection within Ceres' icy mantle predicts an asymmetric heat flow and upwelling of sub-surface material as large-scale cryomagmatic plumes (King et al., 2016). A geomorphic analysis of the Samhain Catenae suggests that the sub-surface Samhain fractures formed due to the uplift and extension of an upwelling region (Scully et al., 2016). Given the location of Samhain Catenae relative to Hanami Planum, Scully et al., (2016) determined that the subsurface buoyancy-driven anomaly suggested by the negative Bouguer gravity (Ermakov et al., 2017), could possibly be evidence for the upwelling region (cryomagmatic plume) predicted by King et al., (2016).

6. Conclusions

Geomorphic evidence that the interior of Ceres is ice-rich has been identified around the dwarf planet (Buczkowski et al., 2016). It has been suggested that the Ceres FFCs are a result of cryomagmatic uplift under the crater floors (Buczkowski et al., 2016). It has also been suggested that the Samhain Catenae formed due to the uplift of Hanami Planum due to cryromagmatic plumes (Scully et al., 2016; King et al., 2016). These features are all found within the Ac-9 quadrangle, and are not only consistent with Ceres having an ice-rich interior, but with it having had active cryomagmatism within its history.

Acknowledgments

Support of the Dawn Instrument, Operations, and Science Teams is gratefully acknowledged. This work is supported by grants from NASA through the Dawn project, and from the German and Italian Space Agencies.

References

Abelson, M., Baer, G., Shtivelman, V., Wachs, D., Rax, E., Crouvi, O., Kurzon, I., Yechieli, Y., 2003. Collapse-sinkholes and radar interferometry reveal neotectonics concealed within the Dead Sea basin,. Geophys. Res. Lett. 30 (10), 1545. doi:10.1029/2003GL017103.

Ammannito, E., et al., 2016. Distribution of phyllosilicates on Ceres. Science 353. doi:10.1126/science.aaf4279.

Angelier, J., Bergerat, F., Dauteuil, O., Villemin, T., 1997. Effective tension-shear relationships in extensional fissure swarms, axial rift zone of northeastern Iceland. J. Struct. Geol. 19, 673–685.

Asphaug, E., Moore, J.M., Morrison, D., Benz, W., Nolan, M.C., Sullivan, R.J., 1996. Mechanical and geological effects of impact cratering on Ida. Icarus 120, 158–184. doi:10.1006/icar.1996.0043.

Bland, M.T., 2013. Predicted crater morphologies on Ceres: probing internal structure and evolution. Icarus 226, 510–521. doi:10.1016/j.icarus.2013.05.037.

Bray, V.J., Schenk, P.M., Melosh, H.J., Morgan, J.V., Collins, G.S., 2012. Ganymede crater dimensions – Implications for central peak and central pit formation and development. Icarus 217, 115–129. doi:10.1016/j.icarus.2011.10.004.

Buczkowski, D.L., Wyrick, D.Y., Toplis, M., Yingst, R.A., Williams, D.A., Garry, W.B., Mest, S., Kniessel, T., Scully, J.E.C., Nathues, A., DeSanctis, M.C., LeCorre, L., Reddy, V., Hoffmann, M., Ammannito, E., Frigeri, A., Tosi, F., Preusker, F., Roatsch, T., Raymond, C.A., Jaumann, R., Pieters, C.M., Russell, C.T., 2014. The unique geomorphology and physical properties of the Vestalia Terra plateau. Icarus. doi:10.1016/j.icarus.2014.03.035.

Buczkowski, D.L., Schmidt, B., Williams, D.A., Mest, S.C., Scully, J.E.C., Ermakov, A.E., Preusker, F., Schenk, P., Otto, K., Hiesinger, H., O'Brien, D., Marchi, S., Sizemore, H., Hughson, K., Chilton, H., Bland, M., Byrne, S., Schorghofer, N., Platz, T., Jaumann, R., Roatsch, T., Sykes, M.V., Nathues, A., De Sanctis, M.C., Raymond, C.A., Russell, C.T., 2016. The geomorphology of Ceres. Science 353. doi:10.1126/science.aaf4332.

Buczkowski, D.L., Wyrick, D.Y., 2014. Tectonism and magmatism identified on asteroids. Geol. Soc. London Spec. Publ. 401, 423–441.

Buczkowski, D.L., Barnouin-Jha, O.S., Prockter, L.M., 2008. 433 Eros lineaments: global mapping and analysis. Icarus 1, 39–52. doi:10.1016/j.icarus.2007.06.028.

Crown, D.A., Sizemore, H.G., Yingst, R.A., Mest, S.C., Platz, T., Berman, D.C., Schmedemann, N., Buczkowski, D.L., Williams, D.A., Roatsch, T., Preusker, F., Raymond, C.A., Russell, C.T., and the Dawn Science Team, Geologic mapping of the Urvara and Yalode Quadrangles of Ceres, Icarus, in review for this issue.

De Sanctis, M.C, et al., 2015. Ammoniated phyllosilicates with a likely outer solar system origin on (1) Ceres. Nature 528, 241–244. doi:10.1038/nature16172, pmid: 26659184.

De Sanctis, M.C., Raponi, A., Ammannito, E., Ciarniello, M., Toplis, M.J., McSween, H.Y., Castillo-Rogez, J.C., Ehlmann, B.L., Carrozzo, F.G., Marchi, S., Tosi, F., Zambon, F., Capaccioni, F., Capria, M.T., Fonte, S., Formisano, M., Frigeri, A., Giardino, M., Longobardo, A., Magni, G., Palomba, E., McFadden, L.A., Pieters, C.M., Jaumann, R., Schenk, P., Mugnuolo, R., Raymond, C.A., Russell, C.T., 2016. Bright carbonate deposits as evidence of aqueous alteration on (1) Ceres. Nature 536, 54–57. doi:10.1038/nature18290.

Dombard, A.J., Gillis, J., 2001. Testing the viability of topographic relaxation as a mechanism for the formation of lunar floor-fractured craters. J. Geophys. Res 106 (27), 901–927. doi:10.1029/2000JE001388, 909.

Durham, W.B., Kirby, S.H., Stern, L.A., 1992. Effects of particulate material on the rheology of ice at planetary conditions. J. Geophys. Res. 97, 20883–20897.

Ermakov, A.I., Park, R.S., Zuber, M.T., Smith, D.E., Fu, R.R., Sori, M.M., Raymond, C.A., Russell, C.T., 2017. Regional analysis of Ceres' gravity anomalies. In: Lunar Planet. Sci. Conf. XLVIII abstract #1374.

Ferrill, D.A., Wyrick, D.Y., Morris, A.P., Sims, D.W., Franklin, N.M., 2004. Dilational fault slip and pit chain formation on Mars. GSA Today 14 (10). doi:10.1130/1052-5173(2004)014⟨4:DFSAPC⟩2.0.CO;2.

French B.M. (1998), *Traces of catastrophe: a handbook of shock-metamorphic effects in terrestrial meteorite impact structures, LPI Contribution No. 954*.

Hall, J.L., Solomon, S.C., Head, J.W., 1981. Lunar floor-fractured craters: evidence of viscous relaxation of crater topography. J. Geophys. Res. 86, 9537–9552.

Hiesinger, H., Marchi, S., Schmedemann, N., Schenk, P., Pasckert, J.H., Neesemann, A., O'Brien, D.P., Kneissl, T., Ermakov, A.I., Fu, R.R., Bland, M.T., Nathues, A., Platz, T., Williams, D.A., Jaumann, R., Castillo-Rogez, J.C., Ruesch, O., Schmidt, B., Park, R.S., Preusker, F., Buczkowski, D.L., Russell, C.T., Raymond, C.A., 2016. Cratering on Ceres: implications for its crust and evolution. Science 353. doi:10.1126/science.aaf4759.

Horstman, K.C., Melosh, H.J., 1989. Drainage pits in cohesionless materials: Implications for the surface of Phobos. J. Geophys. Res 94, 12433–12441.

Jaumann, R., Williams, D.A., Buczkowski, D.L., Yingst, R.A., Preusker, F., Hiesinger, H., Schmedemann, N., Kneissl, T., Vincent, J.B., Blewett, D.T., Buratti, B.J., Carsenty, U., Denevi, B.W., De Sanctis, M.C., Garry, W.B., Keller, H.U., Kersten, E., Krohn, K., Li, J.-Y., Marchi, S., Matz, K.D., McCord, T.B., McSween, H.Y., Mest, S.C., Mittlefehldt, D.W., Mottola, S., Nathues, A., Neukum, G., O'Brien, D.P., Pieters, C.M., Prettyman, T.H., Raymond, C.A., Roatsch, T., Russell, C.T., Schenk, P., Schmidt, B.E., Scholten, F., Stephan, K., Sykes, M.V., Tricarico, P., Wagner, R., Zuber, M.T., Sierks, H., 2012. Vesta's shape and morphology. Science 336, 687.

Jozwiak, L.M., Head, J.W., Zuber, M.T., Smith, D.E., Neumann, G.A., 2012. Lunar floor-fractured craters: classification, distribution, origin and implications for magmatism and shallow crustal structure. J. Geophys. Res. 117. doi:10.1029/2012JE004134.

Jozwiak, L.M., Head, J.W., Wilson, L., 2015. Lunar floor-fractured craters as magmatic intrusions: geometry, modes of emplacement, associated tectonic and volcanic features, and implications for gravity anomalies. Icarus 248, 424–447.

King, S.D., Bland, M.T., Fu, R., Castillo-Rogez, J., Raymond, C.A., Russell, C.T., 2016. 3D Spherical convection modeling of the interior of Ceres. In: Lunar Planet. Sci. Conf. XLVII abstract #1699.

Krohn, K., Jaumann, R., Stephan, K., Otto, K.A., Schmedemann, N., Wagner, R.J., Matz, K.-D., Tosi, F., Zambon, F., von der Gathen, I., Schulzeck, F., Schröder, S.E., Buczkowski, D.L., Hiesinger, H., McSween, H.Y., Pieters, C.M., Preusker, F., Roatsch, T., Raymond, C.A., Russell, C.T., Williams, D.A., 2016. Cryogenic flow features on Ceres: implications for crater-related cryovolcanism. Geophys. Res. Lett. 43. doi:10.1002/2016GL070370.

Küppers, M., O'Rourke, L., Bockelee-Morvan, D., Zakharov, V., Lee, S., von Allmen, P., Carry, B., Teyssier, D., Marston, A., Muller, T., Crovisier, J., Barucci, M.A., Moreno, R., 2014. Localized sources of water vapour on the dwarf planet (1)Ceres. Nature 505, 525–527.

Li, J.Y., McFadden, L.A., Parker, J.W., Young, E.F., Stern, S.A., Thomas, P.C., Russell, C.T., V. Sykes, M., 2006. Photometric analysis of 1 Ceres and surface mapping from HST observations. Icarus, 182, 143–160. doi:10.1016/j.icarus.2005.12.012.

Martin, E.S., Kattenhorn, S.A., 2014. A history of pit chain formation within Enceladus's cratered terrains suggests a nonsynchronous rotation stress field. In: Lunar Planet. Sci. Conf. XLV abstract #1083.

Martin, E.S., Kattenhorn, S.A., 2013. Probing regolith depths on Enceladus by exploring a pit chain proxy. In: Lunar Planet. Sci. Conf. XLIV abstract #2047.

Michaud, R.L., Pappalardo, R.T., Collins, G.C., 2008. Pit chains on Enceladus: a discussion of their origin. In: Lunar Planet. Sci. Conf. XXXIX abstract #1678.

Moore, J.M., Malin, M.C., 1988. Dome craters on Ganymede. Geophys. Res. Lett. 15, 225–228.

Nathues, A., Hoffmann, M., Schaefer, M., Le Corre, L., Reddy, V., Platz, T., Cloutis, E.A., Christensen, U., Kneissl, T., Li, J.-Y., Mengel, K., Schmedemann, N., Schaefer, T., Russell, C.T., Applin, D.M., Buczkowski, D.L., Izawa, M.R.M., Keller, H.U., O'Brien, D.P., Pieters, C.M., Raymond, C.A., Ripken, J., Schenk, P.M., Schmidt, B.E., Sierks, H., 2015. Sublimation in bright spots on (1) Ceres. Nature 528, 237–240. doi:10.1038/nature15754, pmid: 26659183.

Okubo, C., Martel, S., 1998. Pit crater formation on Kilaeua volcano, Hawaii. J. Volcanol. Geotherm. Res. 86, 1–18.

Preusker, F., et al., 2016. Dawn at Ceres – Shape model and rotational state. In: Lunar Planet. Sci. Conf. XXXIV abstract #1954.

Russell, C.T., Raymond, C.A., 2011. The Dawn mission to Vesta and Ceres. Space Sci. Rev. 163, 3–23.

Russell, C.T, et al., 2016. Dawn arrives at Ceres: exploration of a small, volatile-rich world. Science 353, 1008–1010.

Schenk, P.M., 1993. Central pit and dome craters: exposing the interiors of Ganymede and Callisto. J. Geophys. Res. 98, 7475–7498.

Schenk, P., Marchi, S., O'Brien, D., Otto, K., Jaumann, R., Williams, D., Raymond, C., Russell, C.T., 2015. Impact craters on Ceres: evidence for water-ice mantle? In: Euro. Planet. Sci. Congress abstract #EPSC2015-400.

Schenk, P., Marchi, O'Brien, D.P., Bland, M., Platz, T., Hoogenboom, T., Kramer, G., Schröder, S., de Sanctis, M., Buczkowski, D., Sykes, M., McFadden, L.A., Ruesch, O., Le Corre, L., Schmidt, B., Hughson, K., Russell, C.T., Scully, J., Raymond, C., 2016. Impact cratering on the small planets Ceres and Vesta: S-C transitions, central pits and the origin of bright spots. In: Lunar Planet. Sci. Conf. XLVII abstract #2697.

Schultz, P.H., 1976. Floor-fractured lunar craters. The Moon 15, 241–273.

Scully, J.E.C., Buczkowski, D.L., King, S.D., Castillo, J.C., Schmedemann, N., Raymond, C.A., O'Brien, D.P., Raymond, C.A., Marchi, S., Russell, C.T., Mitri, G., Bland, M., 2016. The surface and interior and evolution of Ceres revealed by analysis of fractures and secondary crater chains using Dawn data. Amer. Geophys. Union 2016 Fall Meeting, abs. P54A-05.

Sierks, H., Keller, H.U., Jaumann, R., Michalik, H., Behnke, T., Bubenhagen, F., Buttner, I., Carsenty, U., Christensen, U., Enge, R., Fiethe, B., Gutierrez Marques, P., Hartwig, H., Kruger, H., Kuhne, W., Maue, T., Mottola, S., Nathues, A., Reiche, K.-U., Richards, M.L., Roatsch, T., Schroder, S.E., Szemerey, I., Tschentscher, M., 2011. The Dawn framing camera. *Space Sci. Rev.* 163, 263–327.

Sigurdsson, O., 1980. Surface deformation of the Krafla fissure swarm in two rifting events. J. Geophys. Res. 47, 154–159.

Sims, D.W., Morris, A.P., Ferrill, D.A., Wyrick, D.Y., Colton, S.L., 2003. Physical models of pit chain formation over dilational faults on Mars. In: Lunar Planet. Sci. Conf. XXXIV abstract #2099.

Thomas, N., Barbieri, C, et al., 2012. The geomorphology of (21) Lutetia: results from the OSIRIS imaging system onboard ESA's Rosetta spacecraft. Planet. Space Sci. 66, 96–124. http://dx.doi.org/10.1016/j.pss.2011.10.003.

Yingst, R.A., Mest, S.C., Berman, D.C., Garry, W.B., Williams, D.A., Buczkowski, D., Jaumann, R., Pieters, C.M., De Sanctis, M.C., Frigeri, A., Le Corre, L., Preusker, F., Raymond, C.A., Reddy, V., Russell, C.T., Roatsch, T., Schenk, P.M., 2014. Geologic mapping of Vesta. Planet. Space Sci 103, 2–23.

Williams, D.A., D.L. Buczkowski, S.C. Mest, J.E.C. Scully (this issue), Introduction: The Geologic Mapping of Ceres, Icarus.

Wyrick, D.Y., Ferrill, D.A., Morris, A.P., Colton, S.L., Sims, D.W., 2004. Distribution, morphology, and origins of Martian pit crater chains. J. Geophys. Res. 109, E06005.